# Deriving a CO$_2$-Permselective Carbon Membrane from a Multilayered Matrix of Polyion Complexes

Xinwei Chen,[†] Kian Guan Khoo,[†] Min Woo Kim,[†] and Liang Hong[†,‡,*]

[†]Department of Chemical & Biomolecular Engineering, National University of Singapore, Singapore 117585, Singapore
[‡]Institute of Materials Research and Engineering, Singapore 117602, Singapore

Ⓢ *Supporting Information*
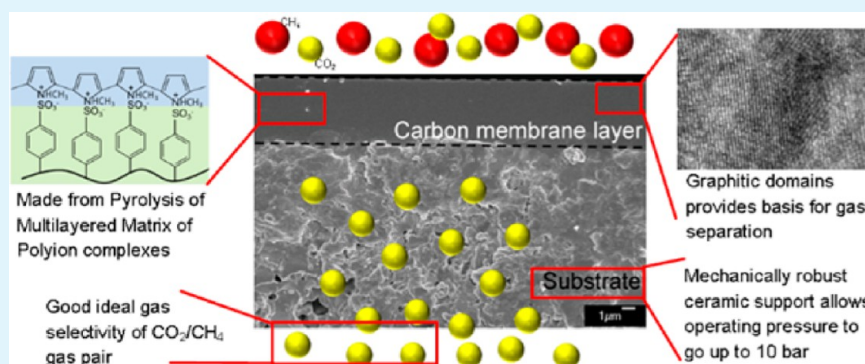
ABSTRACT: A multilayered assembly consisting of polyion complexes was developed over porous ceramic as a unique precursor for a carbon membrane (CM). This specific layer was attained through in situ polymerization of *N*-methylpyrrole (mPy) over a prime coating layer of poly(4-styrenesulfonic acid) (PSSA) with an embedded oxidant on the ceramic surface. Extensive ion-pair complexation between the sulfonic acid groups of PSSA and the tertiary amine groups of the resulting poly(*N*-methylpyrrole) (PmPy) sustains this assembly layer. Incorporating cetyltrimethylammonium bromide (CTAB) into the PSSA is critical in facilitating the infiltration of mPy into the PSSA layer and promoting interfacial contact between the two polymers. Upon pyrolysis, the precursor coating was collectively converted into a carbon composite matrix. Such copyrolysis restrains the grain sizes of the carbonized PmPy, thereby halting defects in the resultant carbonaceous matrix. The gas separation performances of the CMs obtained at various graphitization temperatures showed that the least graphitized carbon matrix exhibited the best selectivity of CO$_2$/CH$_4$ = 167 with a CO$_2$ permeability of 7.19 Barrer. This specific feature is attributed to both imine and imide pendant groups that function as selective adsorption sites for CO$_2$ in the carbon skeleton.

KEYWORDS: layer-by-layer, ceramic support, pyrolysis, conducting polymers, interfacial association

1. INTRODUCTION

Carbon matrixes with extensive triangular planar geometries offer molecular sieving for gas molecules through 3–6-Å pore channels, which are primarily found in the interlayer spacing of graphite and the graphitic domain boundaries.[1,2] The most direct route to the synthesis of a carbon membrane (CM) is through pyrolysis, a process in which a polymeric thin film is heated in an inert environment using a well-designed temperature−time profile until a carbon matrix is formed. The technology was summarized in a recent review article.[3] Thermosetting resins, such as phenolic resins,[4] are often preferred because of their thermal stability at high temperatures. This type of cross-linked polymer experiences a smaller degree of mass elimination during pyrolysis, which consequently prevents the formation of irregular aggregation of polycyclic aromatic hydrocarbons (PAHs) and sp^3 backbones. Otherwise, the resulting pyrolyzed matrix would be highly meso-/macroporous and incapable of achieving gas separation. Similarly, polyimide-based polymers[5−7] and polyfurfuryl alcohol[8−10] have been selected as other possible types of

precursor for CMs, as they suffer minimal mass elimination even at a temperature of 500 °C and are able to provide the desired carbon matrixes to obtain high gas separation performance. Recent advances in exploring graphene and graphene oxide membranes[11,12] manifest high separation factors of 900 for H$_2$/N$_2$ and >2000 for H$_2$/CO$_2$ with permeances for H$_2$ reaching ∼1000 × 10^{-10} mol·m^{-2}·s^{-1}·Pa^{-1}. These separation performances place such membranes higher than the upper boundary line in the Robeson plots for these gas pairs. However, these superthin membranes still lack sufficient adhesion to the ceramic substrate,[12] and solving this problem will promote the viability of their industrial application under harsh conditions. Thus far, the most viable way of making CMs with sufficient mechanical strength to withstand industrial application conditions is to
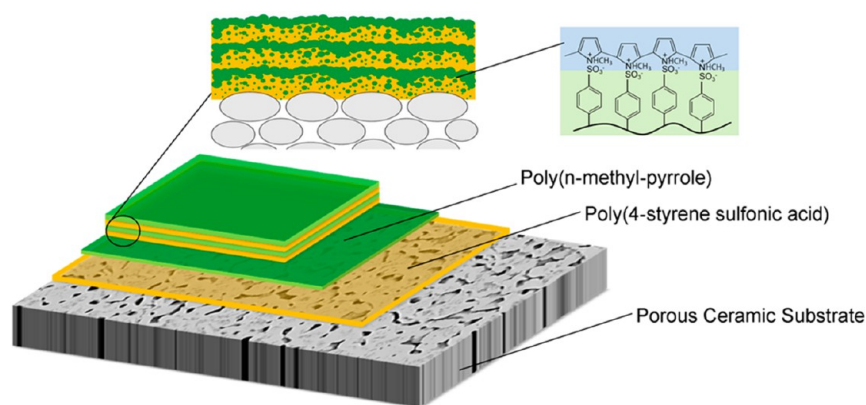
Figure 1. Schematic of the sequential fabrication of a layered polymer assembly formed by ion pairing between poly(N-methyl pyrrole) and poly(4-styrenesulfonic acid) on a porous ceramic substrate.

fabricate a thin layer of CM on a porous ceramic/metal support, commonly known as asymmetric CM.[4,13−15]

Polymers with π-conjugated backbones offer an alternative type of precursor for CMs, unlike those that are known, because such rigid carbon skeletons are structurally closer to PAHs and hence involve a more straightforward thermal degradation path. As a result, complete carbonization can be realized at a relatively low temperature (<600 °C). Conducting polymers with repeating heterocyclic rings such as polypyrrole, polyfuran, polythiophene, and polyaniline are most attractive because the heteroatoms in the conjugated backbone could be retained in the form of different functional groups in the carbon matrix of the CM[16] by tuning the pyrolysis temperature and atmosphere. It is thus likely that the resulting CM could display improved performance for separating gas molecules with similar kinetic diameters through differences in intermolecular affinities rather than molecular size. Hence, the drawback associated with the sieving mechanism, which has reached its Robeson upper bound,[4,17] could be overcome. Indeed, assimilation of inorganic oxide clusters as the extrinsic affinity site in the carbon matrix of a CM represents an advancement in enhancing gas separation performance in the past few years.[18,19] Attempting to incubate an appropriate extent of graphitic domains and pendant nitro groups in the carbon matrix as affinity sites, we are pursuing a polypyrrole-derived carbon matrix because its conjugated structure would give a lower temperature to complete carbonization, which would then preserve the desired nitro groups.

It is well-known that conjugated polypyrrole (PPy) chains have a strong tendency to aggregate together driven by π-affiliation, often leading to the formation of hard granules. Therefore, it is impossible to fabricate a homogeneous carbon matrix starting from such an intact powder by either dissolving it in a solvent or melting it. This dilemma was partially overcome by attaching dodecylbenzenesulfonic acid (DBSA) chains to a portion of the monomer units of PPy chains.[20] The resultant branched chain structure obstructs the stacking of PPy chains and renders the DBSA−PPy chains soluble in protonic aromatic organic solvents, in particular, m-cresol. The film cast on a porous ceramic substrate was homogeneous and, therefore, could be securely transformed into a continuous dense carbon matrix suitable for gas separation applications. However, this route does not utilize the instant polymerization trait of pyrrole (Py) to allow in situ generation of a PPy film directly on the surface of a porous ceramic substrate. The proposed fabrication route in this study aims to eliminate the evaporation step of toxic cresol.

This route starts with the polymerization of mPy, a less reactive monomer than Py. A PSSA coating layer that entraps a polymerization oxidant is first created as a base layer, after which a liquid mPy layer is spread over it for carrying out the in situ polymerization that results in the formation of an overlying PmPy matrix. The PSSA layer provides pendant sulfonic acid groups that associate with the tertiary amine of mPy molecules through ion-pair complexation and with PmPy after the polymerization.[21−23] The anchorage of PmPy to PSSA significantly represses the stacking of the conjugated PmPy chains to form hard grains. This is favorable because such a fine-grained PmPy coating always gives rise to a highly porous carbon matrix that is unsuitable for separating gases. In short, this design leads to an interpenetrating layered assembly consisting of polyion complexes, as illustrated in Figure 1. In addition, no organic solvent is required for such a fabrication route to achieve a uniform and nonporous conducting polymer coating.

The presence of multiple grafting sites [>N$^+$(CH$_3$)H·O$^-$S(═O)$_2$—] between the PmPy and PSSA layers strongly affects the pyrolysis of the PmPy layer. This is because large amounts of free-radical species, which are produced in the PSSA matrix through the swift elimination of sulfonic acid groups in the initial stage of pyrolysis,[24,25] simultaneously couple with the overlying PmPy layer before they start to decompose. Furthermore, as the PSSA-inherited polymer network remains stable until 600 °C, it could therefore buffer against the stress generated in the carbonizing PmPy layer along with cohesion. This unique copyrolysis of the laminar polymer composite hence assures that a uniform and dense matrix is eventually obtained.

On the basis of the proposed protocol, we achieved an asymmetric dense CM with a thickness of a few micrometers on a flat and porous ZrO$_2$-based ceramic substrate. It manifested a mixed mass-transfer mechanism including molecular adsorption, surface diffusion, and Knudsen diffusion during the gas separation assessment. The microstructures of the CM, characterized by graphitic domains, boundary areas between the graphitic domains, and pendant oxy and nitro functional groups on the carbon backbone, could be adjusted primarily by the carbonization temperature. More critically, the incubation of the specific organic functional groups rather than the conventional molecular sieving channels is vital to the effective separation of CO$_2$ from CH$_4$.

2. EXPERIMENTAL SECTION

2.1. Porous Ceramic Membrane with Intermediate Coating. A porous yttria-stabilized zirconia (YSZ) pellet with high permeability and

good mechanical properties was fabricated using the in situ pore-forming technique described elsewhere.[26−28] An intermediate thin modification layer of the same material was then developed through sol−gel coating on the YSZ substrate. This was necessary to prevent an uneven distribution of mass density in the precursor polymer coating developed on the surface of the YSZ substrate because of different capillary effects. A sol−gel coating solution was formulated by the following procedure: 5 mL of zirconium(IV) butoxide in butanol (80%, Aldrich, Milwaukee, WI) was diluted in 18.5 mL of butanol (Aldrich). This solution was subsequently mixed with 0.334 mL of acetyl acetone (Aldrich) and 15 mL of butanol. The resultant solution was blended with a preprepared solution containing 0.239 g of yttrium nitrate (Aldrich) in 15 mL of butanol. Finally, 1.96 mL of deionized water was slowly introduced into this solution under vigorous agitation until a colloidal dispersion composed of $Zr_xY_{1−x}(OH)_y$ sol particles formed.

Slip casting of the colloidal dispersion on the YSZ substrate followed by drying at 75 °C for 30 min was repeated three times. The resulting sol−gel coating was heated in air to 1100 °C at a rate of 2.5 °C/min and held at this temperature for 2 h. After the sample had been cooled at the same rate, the second sol−gel coating was laid down, and the final dwelling temperature was set at 1200 °C at the same heating rate and dwelling duration. The sol−gel-coated pellet was then polished with a P2500 C−Si grinding paper (Buehler) and micropolishing clothes until the surface was smooth and shiny. Finally, the pellet was cleaned by ultrasonication in ethanol to remove the remaining fine powder for applying the PSSA coating. Figure S1 (Supporting Information) shows a comparison of the surfaces of a pristine ceramic support and its counterpart after mechanical polishing.

2.2. Formulation of PSSA-Based Coating Solution for the Development of Prime Layer. Poly(sodium 4-styrenesulfonate) (PSSNa, $M_w ≈ 70000$ g/mol, Aldrich), acidic ion-exchange resin (Amberjet 1200 H ion-exchange resin, Aldrich), ammonium peroxodisulfate (APS; Merck, Darmstadt, Germany), and cetyltrimethylammonium bromide (CTAB, Aldrich) were used to develop the desired prime coat. An aqueous solution of PSSNa (0.1 g/mL) was passed through a column filled with the Amberjet acidic ion-exchange resin twice to allow for complete ion exchange between Na^+ and H^+. The acidified polymer solution, in which PSSNa was converted to PSSA (~0.1 g of PSSA/mL of H_2O), was used to prepare the following three solutions: (i) PSSA−APS solution (0.8 g of APS dissolved in 10 mL of PSSA solution), (ii) PSSA(Na)−APS solution [0.3 mL of PSSNa solution (0.1 g of PSSNa/mL of H_2O) mixed with 9.7 mL of PSSA solution, to which 0.8 g of APS was then added], and (iii) PSSA−CTAB−APS solution (0.18 g of CTAB and 0.8 g of APS dissolved in 10 mL of PSSA solution, such that the calculated molar ratio of styrenesulfonate acid (SSA) monomer units to CTAB was approximately 10).

2.3. In Situ Polymerization of mPy on Top of the PSSA Prime Coat. The pellet obtained from the procedure described in section 2.1 was spin-coated first with PSSA−APS solution, then with PSSA(Na)−APS solution, and finally with PSSA−CTAB−APS solution. Each solution was spin-coated according to a spinning profile of 100 rpm for 10 s followed by 1000 rpm for 30 s, and the resulting liquid film was dried at 75 °C for 15 min before application of the next coating solution. A PSSA prime coat was thus developed in which the imbedded APS was ready for the polymerization of mPy. Onto this prime coat layer was dripped approximately 0.4 mL of mPy (Aldrich), which was left undisturbed for about 15 min to allow for penetration and polymerization. The as-developed PmPy layer was dried under a stream of hot air for 5 min and then in an oven at 75 °C for 15 min. A coating of the PSSA−PmPy assembly was thus realized. After that, the coating was topped by two more such assembly layers to complete the preparation of the precursor, where the polymerization of mPy was extended to 1 h. A control without CTAB was prepared to investigate the effect of the cationic surfactant on the carbon membrane structure.

2.4. Conversion of the PSSA−PmPy Assembly to a Carbon Membrane. The PSSA−PmPy assembly (or precursor coating) was heated to a pyrolysis temperature of interest in the range from 500 to 900 °C using a heating rate of 3 °C/min and a dwelling time of 2 h at the highest pyrolysis temperature. The process was carried out in a tubular

furnace under an argon flow of 30 L/h. The label CM_x is used in this article to denote a carbon membrane where x represents the pyrolysis temperature (°C). For instance, CM_600 specifies a pyrolysis temperature of 600 °C for 2 h. The control sample that was prepared without using CTAB is labeled with a superscript c, namely, CM^c_x. After the first carbon layer had been obtained, the same fabrication procedure was repeated twice to obtain a carbon membrane with a suitable matrix density and mechanical strength for gas separation applications.

2.5. Structural Characterizations. The variation of the glass transition behavior of the PSSA prime coat due to the inclusion of Na^+ and CTAB cations was scrutinized by differential scanning calorimetry (DSC; modulated DSC 2910, TA Instruments, New Castle, DE) at a heating rate of 5 °C/min in flowing nitrogen. The first scan, consisting of heating from 25 to 110 °C and then cooling to 25 °C, was conducted to remove the different thermal histories of the sample, and the thermal response data were recorded during the subsequent scan. In addition, the thermal degradation profiles of the PmPy top coat and the PmPA−PSSA assembly were obtained by thermogravimetric analysis (TGA, DTG-60AH, Shimadzu, Singapore) at a heating rate of 3 °C/min under a N_2 purge of 100 mL/min. The organic functional groups in the carbonaceous materials were determined by Fourier transform infrared (FT-IR) spectroscopy (Bio-Rad FTS-3500ARX, Excalibur Series, Cambridge, MA).

The carbon membranes formed at different fabrication stages were examined by field-emission scanning electron microscopy (FESEM; JEOL JSM-6700F, Tokyo, Japan) to clarify their microstructures. The samples were surface-coated with Pt before FESEM in a platinum coater (JEOL JFC-1300) for charge dissipation purposes. In addition, the carbon membrane structure was examined by transmission electron microscopy (TEM; JEOL 2000FXII). A small piece of carbon membrane was carefully peeled from the ceramic support using a surgical knife and placed in ethanol. After vigorous dispersion in a bath ultrasonicator for 20 min, the suspension was allowed to stand for another 15 min to ensure that the heavier carbon flakes settled. A few drops of the supernatant liquid containing very thin and tiny carbon flakes were transferred onto a TEM copper grid by dripping and drying.

The binding energy values of the N atoms in the substituted amine groups of the carbon skeleton were determined by X-ray photoelectron spectroscopy (XPS; Kratos AXIS His system, Manchester, U.K.) using soft Al $K_α$ X-rays (1486.6 eV). The carbon membrane was mounted on a standard sample holder using double-sided adhesive tape. All core-level spectra were referred to the C 1s neutral carbon peak at 284.6 eV and were curve-fitted by Gaussian component peaks.

In addition, a cross-polarization magic-angle-spinning (CP/MAS) ^{13}C solid-state nuclear magnetic resonance (NMR) study of the carbon structure in the membrane was conducted on a Bruker AVANCE 400 WB spectrometer (Bruker, Karlsruhe, Germany) at 500 MHz and ambient probe temperature. The analysis displayed different carbon environments that varied with the preparation conditions.

2.6. Evaluation of Gas Permeation. The gas-transport characteristics of the resultant carbon membranes were studied by measuring the permeability and hence the selectivity of highly pure single gases with similar kinetic diameters: H_2 (2.89 Å), CO_2 (3.3 Å), O_2 (3.46 Å), N_2 (3.64 Å), and CH_4 (3.8 Å). The gas permeability through the membranes was measured using a constant-volume and variable-pressure setup similar to that used in our previous study.[20] The feed-side pressure was held constant at 90 psi, whereas the permeate-side pressure was kept under a high vacuum for the measurements. A circular area (diameter = 0.8 cm) of the carbon membrane formed on the YSZ pellet (diameter = 2.2 cm) was randomly selected to conduct the gas permeation experiments. The remaining area of the carbon membrane was covered with aluminum adhesive tape (Nashua Aluminum Waterproofing Foil Tape). The pellet was then placed inside a stainless steel module setup, and its periphery was sealed with aluminum adhesive tape. According to this design, permeation took place through the arbitrarily selected area on the membrane, and the measurements were repeated three times for each gas. With the same membrane, another site was selected to repeat the gas permeation tests by the same procedure. Finally, the measurement of another membrane fabricated under the
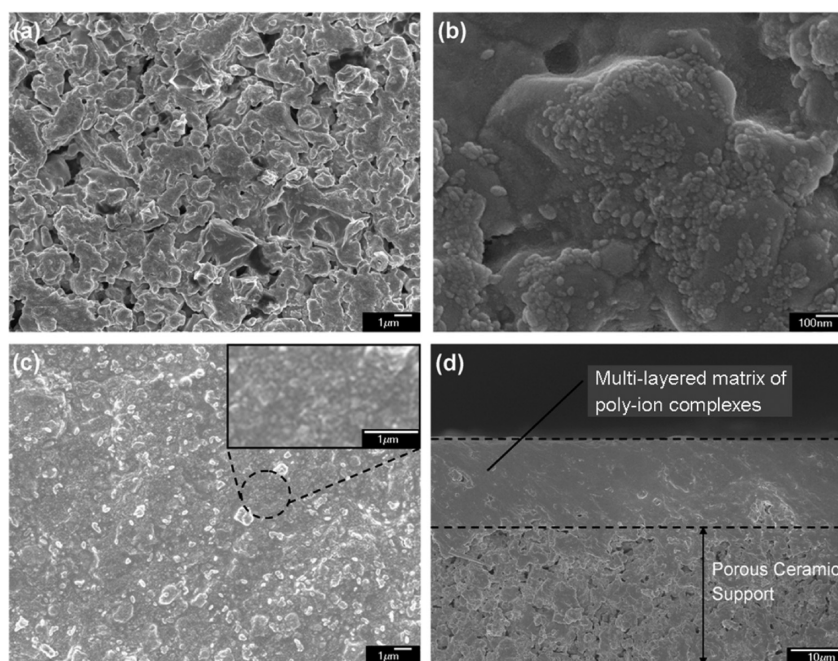
Figure 2. FESEM micrographs of the morphologies of (a) the substrate surface covered by a layer of PSSA prime coat, (b) the same surface at high magnification showing the presence of APS oxidant, (c) the surface after in situ polymerization of mPy, and (d) the cross section of the membrane after in situ polymerization.
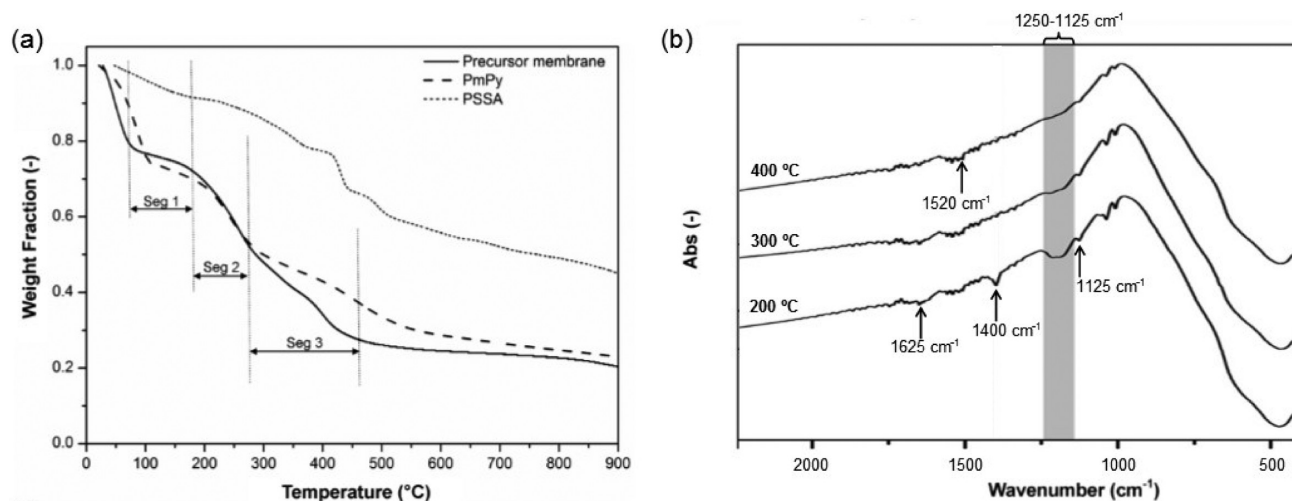

Figure 3. (a) TGA profiles of the PSSA−PmPy precursor coating and the pristine PmPy and PSSA. (b) FT-IR spectra of the pyrolyzed products of the precursor at different temperatures (200, 300, 400 °C) in Ar.

same conditions was carried out. In total, four data sets were obtained to calculate the average pure-gas permeabilities and ideal-gas selectivities.

The gas permeability, P (in Barrer, 1 Barrer = 1×10^{-10} cm^2·s^{-1}·cmHg^{-1}), was determined from the rate of pressure increase (dp/dt) obtained when permeation reached a steady state using the equation

$$P = \frac{dp}{dt}\left(\frac{VT_0 L}{p_0 T \Delta p A}\right)$$

where dp/dt (cmHg·s^{-1}) is the rate of pressure rise at steady state; V (cm^3) is the downstream volume; L (cm) is the membrane thickness; Δp (cmHg) is the pressure difference between the two sides; T (K) is the measurement temperature; A (cm^2) is the effective area of the membrane; and p_0 and T_0 are the standard pressure and temperature, respectively. The ideal separation factor of a membrane for gas A and gas B was evaluated as

$$\alpha_{A/B} = \frac{P_A}{P_B}$$

3. RESULTS AND DISCUSSION

3.1. Thermal Degradation Behavior of the Polymer Precursor Coating. In this study, mPy was used instead of Py in our previous study[15] because of the methyl group of mPy, which sterically discourages intense chain aggregation during polymerization. Instead of being developed directly on the ceramic substrate, a composite polymer layer with the composition PSSA (93%)−PSSNa (1%)−CTAB (6%) was identified to be a chemically relevant substrate (Figure 2a,b) for developing a PmPy layer with a reduced extent of chain aggregation compared with the pristine PmPy. It is rational that this composite substrate (i.e., PSSA layer) provides anchorage for the PmPy polymer
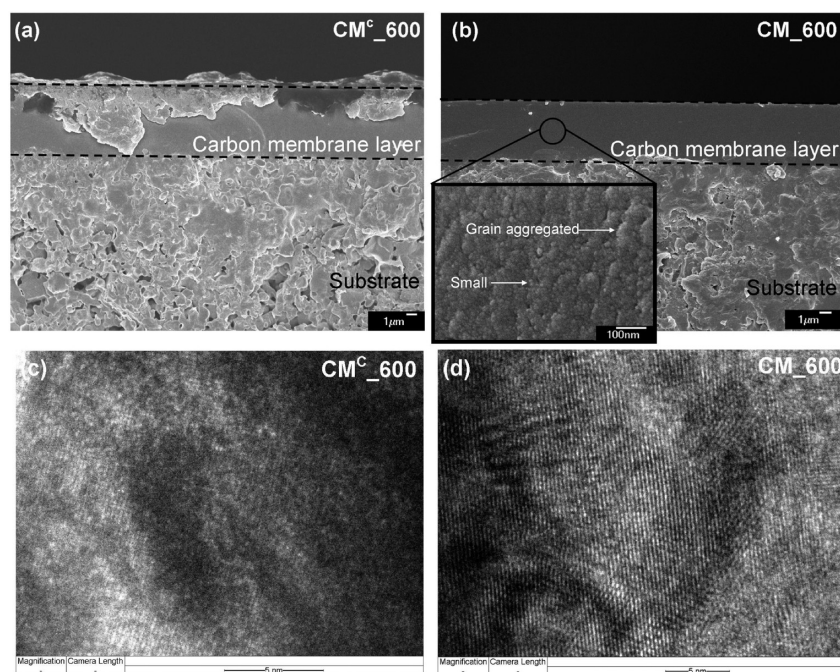
Figure 4. (a,b) Cross-sectional images and (c,d) TEM examinations of carbon membranes (a,c) CM^c_600 and (b,d) CM_600. The inset in panel b shows the details of the microstructure.
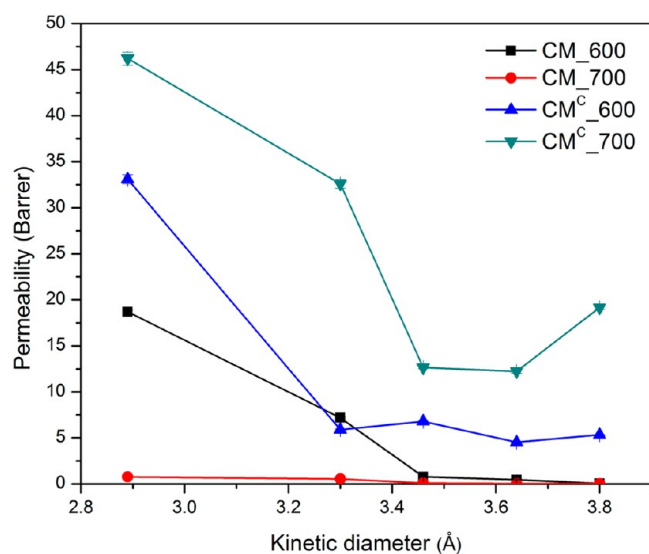

Figure 5. Permeabilities through the prepared carbon membranes of various gases as a function of their molecular sizes.

through ionic pairing of $—SO_3^-·H(CH_3)N^+$ at the interface between the two polymer phases. Figure 2c displays the surface morphology of the PmPy film formed, which comprises predominant miniature grains (<100 nm as sampled by the dashed circle) and some larger lumps with sizes ~1 μm near the surface side. This implies that the formation of polyion complexes hindered the growth of PmPy chains and, hence, resulted in smaller extents of chain aggregation (Figure 2c) compared with the unmodified polymerization of mPy. Detailed in section 2.3, such a polymer assembly was obtained after repeating the procedure three times, and the majority of the PmPy in the polymer coating, according to this sequential addition, was sandwiched between PSSA layers, as illustrated in Figure 1. Finally, a dense multilayer matrix consisting of polyion

complexes (15–20 μm) was obtained as shown in Figure 2d. In addition, this multilayer precursor coating adheres strongly to the porous ceramic support, which is paramount in achieving an asymmetric CM. In the next section, we discuss the fact that a high interfacial contact of PmPy with PSSA is critical to the realization of a qualified carbon membrane.

A comparison of the TGA profiles of pristine PSSA and PmPy with that of the PSSA−PmPy precursor coating provides insight into the pyrolysis behavior of the precursor coating and, more importantly, the variation of thermal behavior of PmPy in the precursor coating (Figure 3a). As reported in the literature,[24] PSSA undergoes the elimination of sulfonic acid groups below 600 °C and produces a stable cross-linked polymer structure. Although PmPy is more thermally vulnerable than PSSA, the PmPy-PSSA precursor displays an even more thermally reactive characteristic than PmPy, as observed in the segment 3 of the TGA profile (Figure 3a). This outcome supports copyrolytic reactions between PmPy and PSSA because of their high interfacial contact, leading to faster formation of carbonaceous material than either component could provide alone. This copyrolysis halts the strong granulation tendency of the carbon generated from the pyrolysis of PmPy and, hence, prevents structural defects caused by the formation of large carbon grain aggregates. Furthermore, the TGA profile of the precursor coating levels off after 500 °C, an indication of the completion of the thermal decomposition and degradation of the volatile moieties. Subsequent heating then causes just structural transformation from carbonaceous to graphite domains, which affects the matrix density (or the width of the mass diffusion channels) and, more significantly, the concentration and type of thermally derived nitro groups on the carbon skeleton. Thus, the suitable carbonization temperature for the resulting carbonaceous matrix was examined in the range from 500 to 900 °C.

FT-IR spectra of the pyrolyzed products of the precursor (Figure 3b) further verify the inference of coincident elimination of both moieties for the ion pair (sulfonate, S=O, 1125−1250
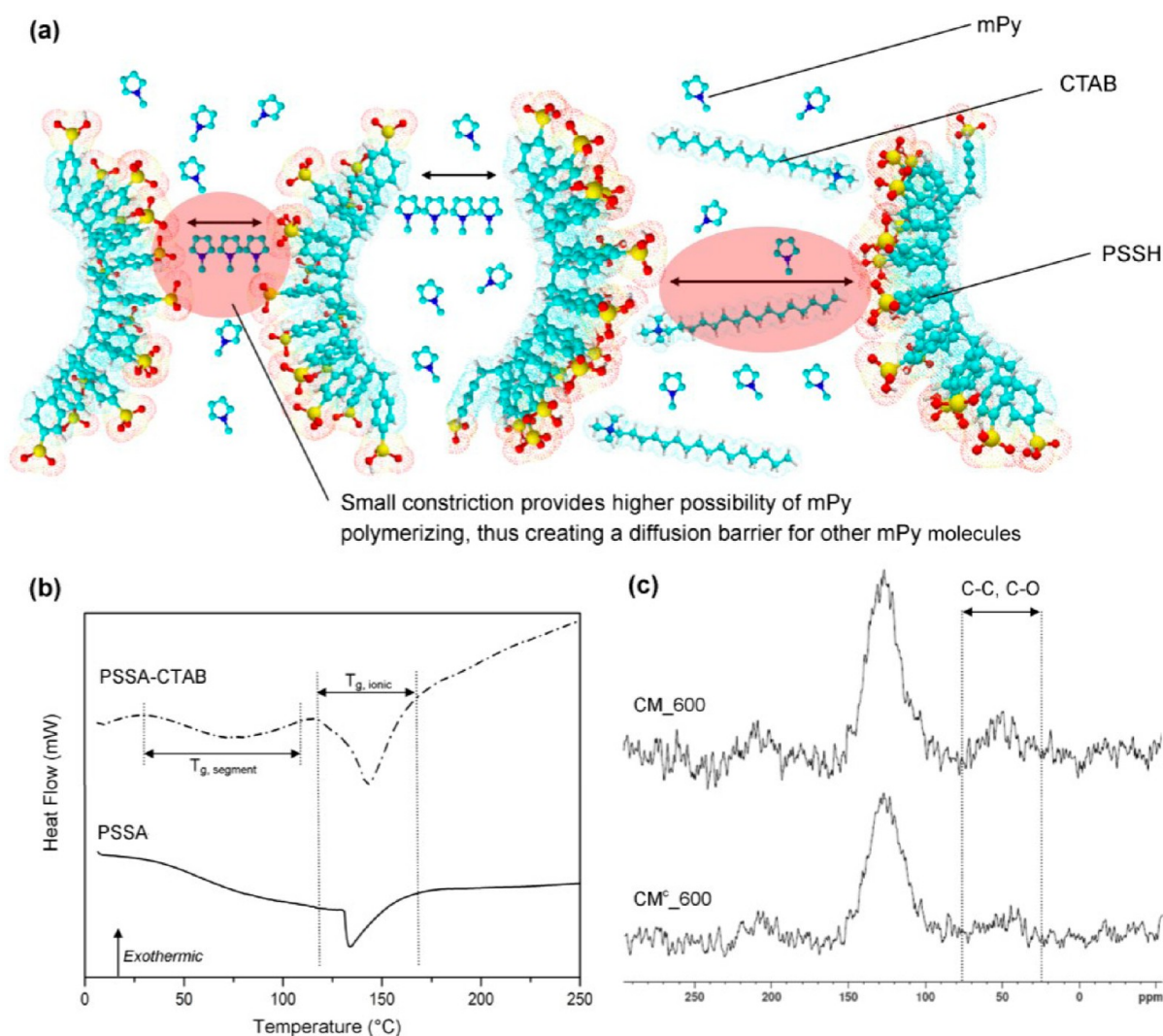
Figure 6. (a) Visualization of the role of CTAB in mediating infiltration of mPy molecules into the PSSA matrix. (b) DSC analysis of the two samples showing their endothermic behaviors. (c) Solid-state C^{13} NMR spectra of the carbon membranes pyrolyzed at 600 °C with and without the addition of CTAB.

cm^{-1}; protonated mPy, C—N, 1000−1125 cm^{-1}) when the pyrolysis temperature was increased from 200 to 400 °C. In addition, almost negligible carboxylic acid (1625 cm^{-1}), formed because of the oxidizing role of SO_3 from the elimination of —SO_3H or APS (oxidant), was detected after 400 °C because of thermal decarboxylation. Concurrently, the emergence of the characteristic aromatic skeleton (1520 cm^{-1}) marks the onset of the growth of PAHs. In addition, the O—H bending (1400 cm^{-1}) attributed to the hydration water of the sulfonic acid groups was not observed when the pyrolysis was carried out at 300 °C, indicating elimination of the sulfonic acid groups.

3.2. Role of CTAB Surfactant in the Evolution of a Uniform Carbon Matrix. It can be identified by inspecting the images in Figure 4a,b that the presence of a small amount of the cationic surfactant CTAB in the precursor coating significantly affects the carbon matrix structure generated. It is presumed that the CM^c_600 membrane without the inclusion of CTAB in the precursor coating contains numerous pits or crevices between carbon grains caused by heavy aggregation that occurs during pyrolysis (Figure 4a). In light of this, CTAB works to facilitate, through the in situ polymerization step, the intercalation of PmPy into the PSSA matrix. This intercalation accordingly

promotes the copyrolysis of the two polymers, which results in substantially small carbonaceous grains. Indeed, the detailed matrix structure of CM_600 (inset of Figure 4b) displays a uniform intermingling of grains with different extents of agglomeration ranging from ∼100 nm (the largest) to <10 nm (the smallest). TEM scrutiny further clarified the structural discrepancy between the two carbon matrixes (Figure 4c,d). Both images display crisp lattice lines representing graphene sheets, which are distinct in CM_600 but not in CM^c_600. Such a difference in microstructures also exists in the other CMs obtained using different pyrolysis temperatures. Furthermore, the gas permeation test displayed results consistent with those of the above microscopic analysis (Figure 5). This confirms that CM_x is denser than CM^c_x obtained at the same pyrolysis temperature (refer also to Table S1, Supporting Information), as the latter matrix presents a lower resistance to the permeation of gas molecules. More critically, the CM^c_x membranes are basically nonselective to gases (Table S2, Supporting Information), indicating the presence of loopholes in their matrixes.

Regarding the role of CTAB, CTAB molecules strongly attach themselves to the PSSA chains by forming ion pairs between a quaternary ammonium group and a pendant sulfonic acid group
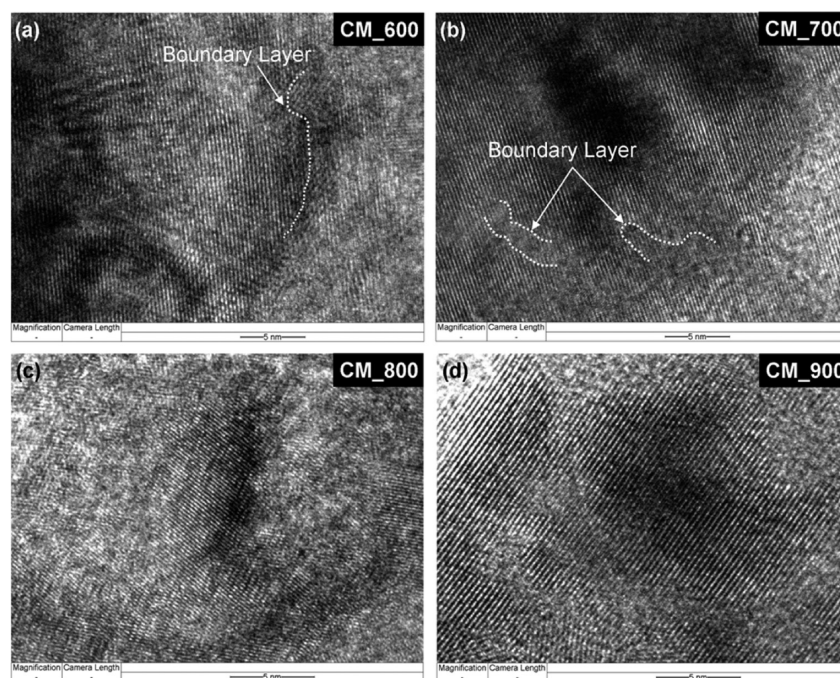
Figure 7. TEM images of the carbon lattice structure in which four membranes with different pyrolysis temperatures were examined.

with elimination of HBr molecules when both are mixed in water.[29] As a result, most of the CTAB molecules stay in the bulk rather than at the surface of the coating during the drying step because of their immobilization state. Thus, the C_{16} hydrocarbon moiety of CTAB acts as a spacer between the PSSA chains. This anchoring weakens nearby hydrogen bonds of the sulfonic acid groups through the spatial distancing effect (Figure 6a). The perturbation caused by the presence of CTAB in the PSSA prime coat matrix is evidenced by DSC analysis (Figure 6b), which shows the segment motion of a loose network within the temperature range $T_{g,segment}$, in contrast to negligible response from the matrix where CTAB is absent. As a result, the CTAB-doped PSSA prime coat matrix permits the infiltration of mPy into the deeper territory of the PSSA matrix because of its looser chain packing density relative to that in the absence of CTAB from the matrix. A larger concentration of mPy in the PSSA matrix assures a higher interfacial contact between the two polymers and, hence, smaller PmPy grain sizes as a result of the steric hindrance effect described previously.

^{13}C NMR spectroscopy provides additional information about the impact of CTAB on the prepared carbon matrix. The ^{13}C NMR spectra (Figure 6c) show that CM_600 contains a greater portion than CM^c_600 of sp^3 carbon species, reflected by the absorption peaks in the chemical shift range of 25−75 ppm. It is likely that CTAB molecules were gradually converted into PAHs during the carbonization process because the CTAB molecules were intimately imbedded in the composite matrix of PSSA and PmPy, as a result of the mPy infiltration and subsequent polymerization in PSSA. Hence, carbonization of the imbedded CTAB molecules is likely to have contributed to the additional sp^3 carbon species. These carbon species mainly include both quaternary carbons ≻C— and heteroatom-substituted tertiary carbons ≻C—X, for example, alcohol or ether. They are often substituted on the edges and facets of PAHs and, hence, would exist on the surfaces of carbon grains and the gaps between PAHs because the surfaces are dominated by the edges of PAHs and fissures or defects among them. It is statistically sound to

conclude that smaller carbon grains would contain a greater number of sp^3 species than larger grains. The higher ^{13}C NMR absorption in the sp^3 carbon region is consistent with the microstructure observed, justifying from another perspective the role of CTAB described above.

3.3. Impact of Carbon Membrane Structure on Gas Separation. The microstructure of CM_600 (Figure 4b) demonstrates that the carbon membrane matrix consists of closely packed carbon grains of which the elementary grains have sizes of a few dozen nanometers. Any such grain, in principle, comprises a few graphitic domains, and this could be characterized by the TEM micrograph taken from an arbitrarily selected grain (Figure 7). There are two types of structural boundaries: those situated between carbon grains and those situated between graphitizing domains. It is known that graphitic domains comprise the alignment of graphene (or PAHs) sheets. As such, a boundary could be identified wherever an alignment pattern of graphene sheets no longer continues, as indicated by dashed lines in panels a and b of Figure 7. Consequently, gas molecules transport along these two kinds of boundary areas and penetrate through the graphitic domains.

The carbon membrane matrix resulting from the PmPy−PSSA assembly could be tuned by varying the highest pyrolysis temperature used, as shown by the variation in gas permeability as a function of pyrolysis temperature in Figure 8a and Table S1 (Supporting Information), which presents a minimum of permeability at 800 °C, followed by a fast rise when the temperature was increased to 900 °C. The CMs pyrolyzed at 500 and 550 °C displayed lower selectivities than their counterparts subjected to higher pyrolysis temperatures despite having higher permeabilities (Figure 8a and Table S2, Supporting Information). Compared with our previous study in which PPy was employed as a precursor for CMs,[20] both CM_500 and CM-500 of the previous work showed similar selectivity values caused mainly by Knudsen diffusion. Additionally, contrary to the previous CM-600 membrane that still retained the same mass-transport mechanism, the present CM_550 membrane showed
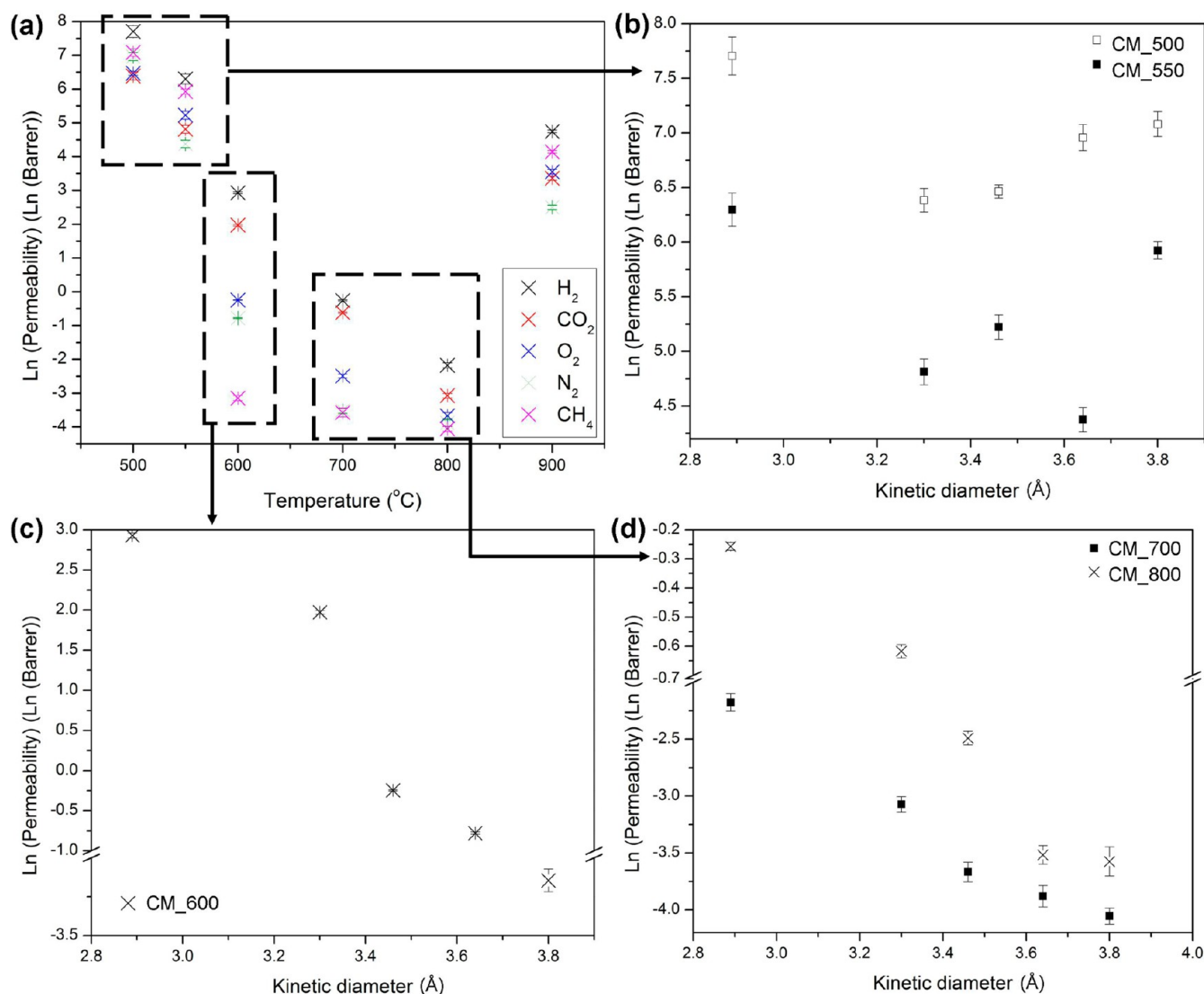
10226

dx.doi.org/10.1021/am5015953 | ACS Appl. Mater. Interfaces 2014, 6, 10220−10230

Figure 8. Gas-transport phenomena of carbon membranes pyrolyzed at different temperatures: Permeabilities of gases as functions of (a) pyrolysis temperature and (b−d) their molecular sizes. A natural logarithm transformation was performed on the permeabilities of the gases to improve the interpretability of the data. Refer to Table S1 (Supporting Information) for details about respective standard deviations.

not only Knudsen diffusion but also the influence of physical adsorption, which is rational given that the two membranes were made from different precursors and by different pyrolysis procedures. Regarding the rest of the CMs, their TEM images show that increasing the highest carbonization temperature from 600 to 700 °C brought about an expansion of the graphitization phase. However, performing carbonization at 800 °C led to a matrix with randomly associated domains. Correspondingly, a small mass loss step appearing at 800 °C was reflected in the TGA profile (Figure 3a). This mass elimination caused a disconnection of the boundary phase that was responsible for the lowest permeability being exhibited by the CM_800 membrane (Figure 8a; Table S1, Supporting Information). Such a random matrix was turned into a well-aligned graphene structure with an intersheet distance of about 0.5 nm after calcination at 900 °C (Figure 7d). An obvious improvement in the permeability but not in the selectivity resulted. This can be attributed to the typical matrix geometry: (1) an intersheet distance in the graphite domains that is relatively broader than the sizes of the gas molecules and (2) an increase in the width of the boundary areas between carbon grains that experience contractions accompany-

ing the increase in graphitization. These two factors explain why the separation factors of N_2/CH_4 and CO_2/CH_4 were less than 1, implying that the molecular weights of the gases become important in transport phenomena. However, it is interesting to note that this membrane showed a separation factor of 2.85 for O_2/N_2 (Table S2, Supporting Information), which was likely affected by the stronger physical adsorption of O_2 because O_2 has a higher critical temperature (T_c) than N_2. The selectivity therefore does not follow the pore diffusivity order determined by the molecular weights of the molecules for Knudsen diffusion. Furthermore, for the CO_2/CH_4 gas pair, the CM_900 membrane permeated CH_4 and exhibited a selectivity factor of 0.456 (Table S2, Supporting Information), which was slightly lower than the typical Knudsen diffusion of 0.62. As for the O_2/N_2 pair, CO_2 is a stickier molecule than CH_4 because of its higher T_c. The physical adsorption effect also explains the separation factors of N_2/CH_4 and H_2/N_2 being beyond what size-dependent diffusion could interpret (Figure 9).

Regarding the separation of the CO_2/CH_4 pair, the CM_600 membrane provided a dramatically improved selectivity among the membranes. Additionally, unlike the CM_550 and CM_900
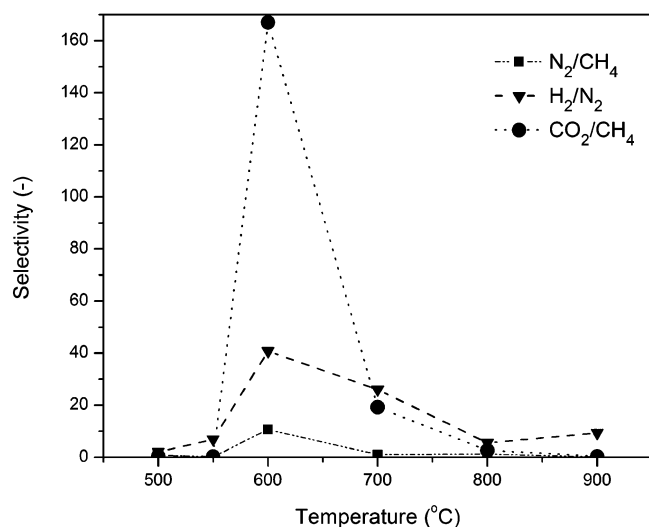
Figure 9. Ideal membrane selectivities for selected gas pairs, showing a clear dependency on the highest pyrolysis temperature used to prepare the CM.

membranes, it permeated CO_2 instead of CH_4. Compared to CM_550, CM_600 exhibited a lower permeability (Figure 8b,c)

and thus must have contained thinner boundary areas. This effectively narrowed the Knudsen diffusion pathway, directing the gas molecules to hop over the selective adsorption sites spread over the two boundaries as previously defined. On the other hane, the CM_700 membrane, having a greater extent of graphitization as shown in Figure 7b, offered a low selectivity to the same pair and lower permeability, presumably because of the loss of the specific adsorption sites along the continuous boundary areas.

To further support this conclusion, N 1s XPS spectra of the above four membranes (Figure 10) were found to show different distributions of the following N-containing organic functional groups: —N═ (pyridine type, 397.6 and 398.2 eV), (—$CO)_2$NR (imide, 399.4 ± 0.3 eV), —C(O)N < (amide type, 400.2 eV), and >N^+< (quaternary ammonium, 401.2 ± 0.3 eV).[30] It can be noted from Figure 10c,d that only the imide functional group could survive the carbonization at 800 and 900 °C, whereas the other N-containing species identified by the deconvolution of the peaks were actually not present. Regarding the N-containing groups, the CM_600 membrane displayed a peak with the lowest N 1s binding energy at 397.6 eV, indicating the presence of the pyridine-type soft Lewis base and a higher portion of imide group (ca. 63.4%) than CM_700. This characterization result suggests that the imide group, because
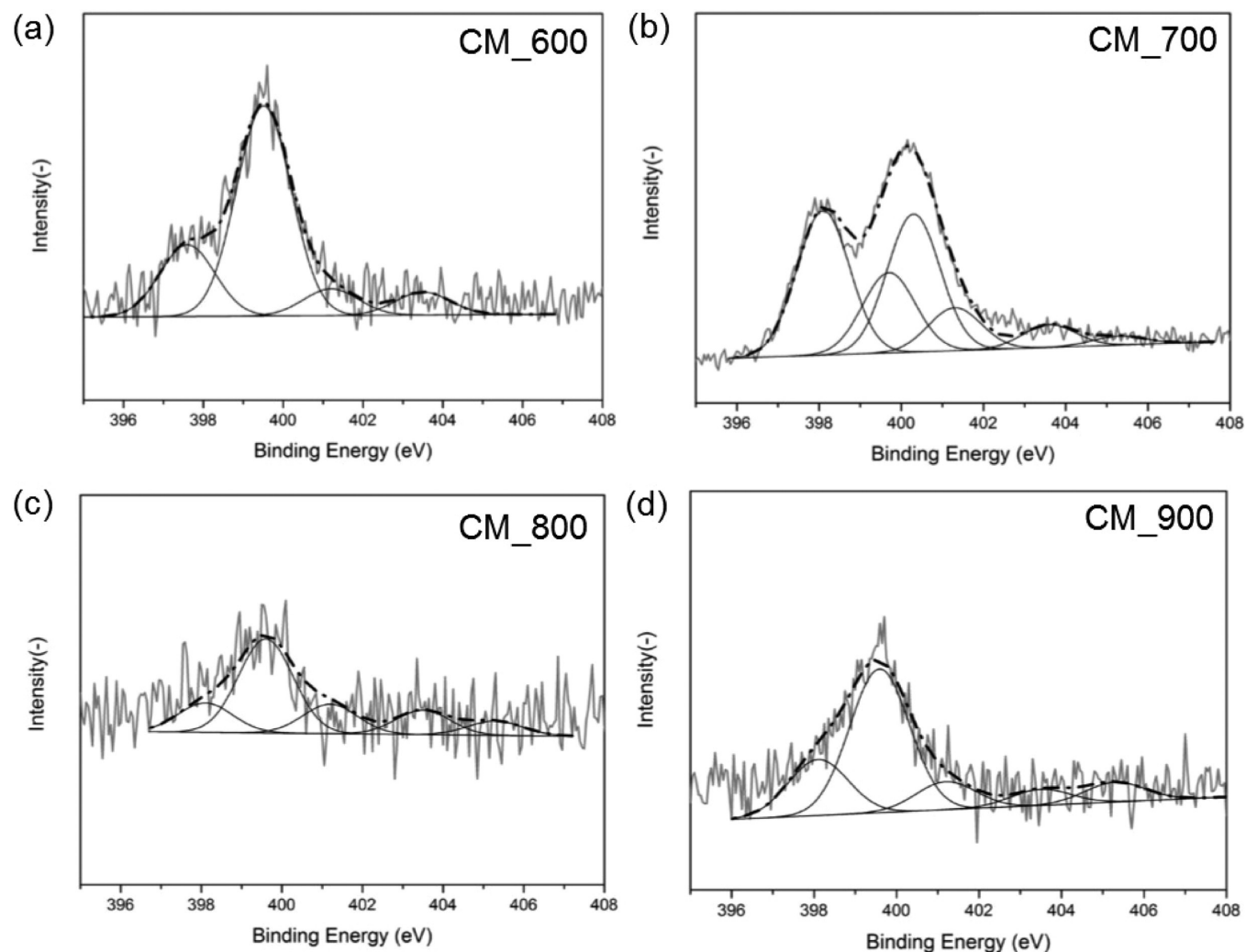

Figure 10. N 1s XPS spectra of the four CMs prepared at different pyrolysis temperatures as labeled.

of its structural similarity to CO_2, provides a suitable hopping site for CO_2. The observation that CM_600 and CM^c_600 displayed similar permeabilities for CO_2 but not for other gases (Figure 5; Table S1, Supporting Information) also suggests the role of the N-containing organic groups that should have similar abundances in the two membranes. This phenomenon has been also noted in polyimide membranes that offer CO_2/CH_4 separation selectivity.[14,31,32] Although both the CM_800 and CM_900 membranes were also found to bear the imide group with concentrations that were insignificantly lower than that of the CM_600 membrane according to the N 1s XPS spectra, their substantially poorer selectivity compared to CM_600 could be attributed to their particular matrix geometry, as elucidated above, as well as a lack of pertinent adsorption sites. The latter structural characteristic also explains the large difference in the CO_2/CH_4 separation factor between CM_600 and CM_700 (Figure 9) because the pyridine group, a softer Lewis base than imide, in CM_600 might play a complementary role in alleviating the affinity of CO_2 for imide and hence favor mass transport. This interaction differs from the normal physical adsorption that hinders the diffusion of adsorbate molecules. Regarding CO_2/CH_4 separation, two recent reviews on polymeric[33] and inorganic[34] membranes showed that both types of membrane could achieve separation factors comparable to that of CM_600 under their best conditions. For instance, zeolite membrane supported on porous Al_2O_3 was found to exhibit a CO_2/CH_4 separation selectivity higher than 170 with a CO_2 permeance at 2.0×10^{-6} mol·m^{-2}·s^{-1}·Pa^{-1}.[35] In general, polymeric membranes are normally vulnerable to H_2S and high pressure, where both carbon and zeolite membranes have advantages. In light of the unsatisfactory aspect of this work, the separation performances of the membranes are based on ideal-gas selectivity (or single-gas permeation). Hence, an investigation into mixed-gas separation will be required to fully comprehend the separation mechanisms of this membrane.

4. CONCLUSIONS

An asymmetric carbon membrane (CM) derived from poly(*N*-methylpyrrole), a conjugated polymer, has been achieved for gas separation. The main findings from the fabrication and characterization of this CM are summarized as follows.

(1) The polymerization of *N*-methylpyrrole (mPy) at the interface with a coating of poly(4-styrenesulfonic acid) (PSSA) enables the formation of a dual-layered assembly that is supported by polyion complexes and mechanical interlocking. This interfacial polymerization is essential to prevent the formation of a granulated PmPy matrix, which is undesirable because such a matrix leads to a highly porous carbon matrix after pyrolytic conversion.

(2) Pre-embedding of the cationic surfactant, CTAB, in the PSSA matrix is crucial to the attainment of a loophole-free carbon matrix for gas separation because CTAB facilitates penetration of the PmPy into the PSSA matrix through the in situ polymerization of mPy.

(3) The PmPy-PSSA assembly completes carbonization at a temperature as low as 500 °C, followed by graphitization at increasing temperature. The CM obtained from pyrolysis at 600 °C manifested the best CO_2/CH_4 permselectivity of 167 with a CO_2 permeability of 7.19 Barrer. This performance is attributed to realizing a tradeoff between graphitizing PAHs and deriving pendant imide groups to provide CO_2 hopping sites in the resulting CM matrix.

The present CM fabrication approach explores the in situ formation of a conjugated polymer matrix and its polyionic complexation with an anionic polymer matrix to assemble a precursor coating for the CM. This dual-polymer assembly permits a carbon matrix that separates gases primarily through the graphitic boundary, where different pendant nitro groups provide selective molecular transport.

■ ASSOCIATED CONTENT

Ⓢ Supporting Information
Additional information as noted in text. This material is available free of charge via the Internet at http://pubs.acs.org.

■ AUTHOR INFORMATION

Corresponding Author
*E-mail: chehongl@nus.edu.sg. Tel.: +65-6516 5029. Fax: +65-6779 1936.

Author Contributions
The manuscript was written through contributions of all authors. All authors have given approval to the final version of the manuscript.

Notes
The authors declare no competing financial interest.

■ ACKNOWLEDGMENTS

■ REFERENCES

(1) Kyotani, T. Control of Pore Structure in Carbon. *Carbon* **2000**, *38*, 269−286.

(2) Suda, H.; Haraya, K. Molecular Sieving Effect of Carbonized Kapton Polyimide Membrane. *J. Chem. Soc., Chem. Commun.* **1995**, 1179−1180.

(3) Salleh, W. N. W.; Ismail, A. F.; Matsuura, T.; Abdullah, M. S. Precursor Selection and Process Conditions in the Preparation of Carbon Membrane for Gas Separation: A Review. *Sep. Purif. Rev.* **2011**, *40*, 261−311.

(4) Centeno, T. A.; Vilas, J. L.; Fuertes, A. B. Effects of Phenolic Resin Pyrolysis Conditions on Carbon Membrane Performance for Gas Separation. *J. Membr. Sci.* **2004**, *228*, 45−54.

(5) Jones, C. W.; Koros, W. J. Carbon Molecular-Sieve Gas Separation Membranes. 1. Preparation and Characterization Based on Polyimide Precursors. *Carbon* **1994**, *32*, 1419−1425.

(6) Hosseini, S. S.; Chung, T. S. Carbon Membranes from Blends of PBI and Polyimides for N_2/CH_4 and CO_2/CH_4 Separation and Hydrogen Purification. *J. Membr. Sci.* **2009**, *328*, 174−185.

(7) Geiszler, V. C.; Koros, W. J. Effects of Polyimide Pyrolysis Conditions on Carbon Molecular Sieve Membrane Properties. *Ind. Eng. Chem. Res.* **1996**, *35*, 2999−3003.

(8) Burket, C. L.; Rajagopalan, R.; Marencic, A. P.; Dronvajjala, K.; Foley, H. C. Genesis of Porosity in Polyfurfuryl Alcohol Derived Nanoporous Carbon. *Carbon* **2006**, *44*, 2957−2963.

(9) Song, C. W.; Wang, T. H.; Jiang, H. W.; Wang, X. Y.; Cao, Y. M.; Qiu, J. S. Gas Separation Performance of C/CMS Membranes Derived from Poly(furfuryl alcohol) (PFA) with Different Chemical Structure. *J. Membr. Sci.* **2010**, *361*, 22−27.

(10) Anderson, C. J.; Pas, S. J.; Arora, G.; Kentish, S. E.; Hill, A. J.; Sandler, S. I.; Stevens, G. W. Effect of Pyrolysis Temperature and Operating Temperature on the Performance of Nanoporous Carbon Membranes. *J. Membr. Sci.* **2008**, *322*, 19−27.

(11) Kim, H. W.; Yoon, H. W.; Yoon, S.-M.; Yoo, B. M.; Ahn, B. K.; Cho, Y. H.; Shin, H. J.; Yang, H.; Paik, U.; Kwon, S.; Choi, J.-Y.; Park, H. B. Selective Gas Transport through Few-Layered Graphene and Graphene Oxide Membranes. *Science* **2013**, *342*, 91−95.

(12) Li, H.; Song, Z.; Zhang, X.; Huang, Y.; Li, S.; Mao, Y.; Ploehn, H. J.; Bao, Y.; Yu, M. Ultrathin, Molecular-Sieving Graphene Oxide Membranes for Selective Hydrogen Separation. *Science* **2013**, *342*, 95−98.

(13) Saufi, S. M.; Ismail, A. F. Fabrication of Carbon Membranes for Gas Separation—A Review. *Carbon* **2004**, *42*, 241−259.

(14) Park, H. B.; Kim, Y. K.; Lee, J. M.; Lee, S. Y.; Lee, Y. M. Relationship between Chemical Structure of Aromatic Polyimides and Gas Permeation Properties of Their Carbon Molecular Sieve Membranes. *J. Membr. Sci.* **2004**, *229*, 117−127.

(15) Kiyono, M.; Williams, P. J.; Koros, W. J. Effect of Polymer Precursors on Carbon Molecular Sieve Structure and Separation Performance Properties. *Carbon* **2010**, *48*, 4432−4441.

(16) Strelko, V. V.; Kuts, V. S.; Thrower, P. A. On the Mechanism of Possible Influence of Heteroatoms of Nitrogen, Boron and Phosphorus in a Carbon Matrix on the Catalytic Activity of Carbons in Electron Transfer Reactions. *Carbon* **2000**, *38*, 1499−1503.

(17) Centeno, T. A.; Fuertes, A. B. Carbon Molecular Sieve Gas Separation Membranes Based on Poly(vinylidene chloride-*co*-vinyl chloride). *Carbon* **2000**, *38*, 1067−1073.

(18) Park, H. B.; Lee, Y. M. Fabrication and Characterization of Nanoporous Carbon/Silica Membranes. *Adv. Mater.* **2005**, *17*, 477−483.

(19) Lie, J. A.; Hägg, M.-B. Carbon Membranes from Cellulose and Metal Loaded Cellulose. *Carbon* **2005**, *43*, 2600−2607.

(20) Chen, X.; Hong, L.; Chen, X. L.; Yeong, W. H. A.; Chan, W. K. I. Aliphatic Chain Grafted Polypyrrole as a Precursor of Carbon Membrane. *J. Membr. Sci.* **2011**, *379*, 353−360.

(21) Arribas, C.; Rueda, D. Preparation of Conductive Polypyrrole-Polystyrene Sulfonate by Chemical Polymerization. *Synt. Met.* **1996**, *79*, 23−26.

(22) De Jesus, M. C.; Weiss, R. A.; Chen, Y. The Development of Conductive Composite Surfaces by a Diffusion-Limited in Situ Polymerization of Pyrrole in Sulfonated Polystyrene Ionomers. *J. Polym. Sci. B: Polym. Phys.* **1997**, *35*, 347−357.

(23) Harada, A.; Kataoka, K. Formation of Polyion Complex Micelles in an Aqueous Milieu from a Pair of Oppositely-Charged Block Copolymers with Poly(ethylene glycol) Segments. *Macromolecules* **1995**, *28*, 5294−5299.

(24) Jiang, D. D.; Yao, Q.; McKinney, M. A.; Wilkie, C. A. TGA/FTIR Studies on the Thermal Degradation of Some Polymeric Sulfonic and Phosphonic Acids and Their Sodium Salts. *Polym. Degrad. Stab.* **1999**, *63*, 423−434.

(25) Yao, Q.; Wilkie, C. A. Thermal Degradation of Blends of Polystyrene and Poly(sodium 4-styrenesulfonate) and the Copolymer, Poly(styrene-co-sodium 4-styrenesulfonate). *Polym. Degrad. Stab.* **1999**, *66*, 379−384.

(26) Chen, X.; Hong, L.; Tai, X. H. Submicron-Scale Exclusion via Polymerizing an Aromatic Nylon in Molded Ceramic Monolith for Paving Interconnected Pore Channels. *J. Am. Ceram. Soc.* **2011**, *94*, 382−390.

(27) Chen, X.; Hong, L. An In Situ Approach to Create Porous Ceramic Membrane: Polymerization of Acrylamide in a Confined Environment. *J. Am. Ceram. Soc.* **2010**, *93*, 96−103.

(28) Chen, X.; Hong, L.; Phua, J. Y. R. Evolution of Throttle-Channel Dual Pores in YSZ Ceramic Monolith through in Situ Grown Nano Carbon Wedges. *J. Eur. Ceram. Soc.* **2012**, *32*, 3709−3722.

(29) Zhou, Y.; Tang, X.; Xu, Y.; Lu, J. Effect of Quaternary Ammonium Surfactant Modification on Oil Removal Capability of Polystyrene Resin. *Sep. Purif. Technol.* **2010**, *75*, 266−272.

(30) Jansen, R. J. J.; Vanbekkum, H. XPS of Nitrogen-Containing Functional Groups on Activiated Carbon. *Carbon* **1995**, *33*, 1021−1027.

(31) Su, J.; Lua, A. C. Effects of Carbonisation Atmosphere on the Structural Characteristics and Transport Properties of Carbon

Membranes Prepared from Kapton® Polyimide. *J. Membr. Sci.* **2007**, *305*, 263−270.

(32) Tin, P. S.; Xiao, Y. C.; Chung, T. S. Polyimide-Carbonized Membranes for Gas Separation: Structural, Composition, and Morphological Control of Precursors. *Sep. Purif. Rev.* **2006**, *35*, 285−318.

(33) Zhang, Y.; Sunarso, J.; Liu, S.; Wang, R. Current Status and Development of Membranes for CO_2/CH_4 Separation: A Review. *Int. J. Greenhouse Gas Control* **2013**, *12*, 84−107.

(34) Pera-Titus, M. Porous Inorganic Membranes for CO_2 Capture: Present and Prospects. *Chem. Rev.* **2013**, *114*, 1413−1492.

(35) Carreon, M. A.; Li, S.; Falconer, J. L.; Noble, R. D. Alumina-Supported SAPO-34 Membranes for CO_2/CH_4 Separation. *J. Am. Chem. Soc.* **2008**, *130*, 5412−5413.

10230

dx.doi.org/10.1021/am5015953 | *ACS Appl. Mater. Interfaces* 2014, 6, 10220−10230